Resources, Conservation & Recycling 164 (2021) 105166

Contents lists available at ScienceDirect

Resources, Conservation & Recycling

journal homepage: www.elsevier.com/locate/resconrec

Full length article

Development of zero cement composite for the protection of concrete sewage pipes from corrosion and fatbergs

Rajeev Roychand*, Jie Li, Saman De Silva, Mohammad Saberian, David Law, Biplob Kumar Pramanik

School of Engineering, RMIT University, Melbourne, VIC 3000, Australia

ARTICLE INFO

Keywords:
nano-silica
slag, fly-ash
concrete corrosion
fatbergs
concrete sewage pipes

ABSTRACT

The pursuit of environmental friendly alternatives for ordinary Portland cement (OPC) finds increased attention when the latter poses serious durability issues in major infrastructure applications, such as sewage drainage pipes. The presence of large quantities of free lime in OPC concrete used in the manufacturing of sewage pipes, exposes them to (i) concrete corrosion in acidic sewage environment, and (ii) clogging of sewage network due to the formation of calcified fatbergs. There appears to be very limited or no research on the development of an eco-friendly zero cement composite that can protect the concrete sewage pipes from corrosion and can eliminate the free lime that contributes towards the formation of fatbergs. Therefore, to address this research gap, an experimental investigation was undertaken on quaternary blended cement composites containing nano-silica, fly-ash, slag, and hydrated lime. These cement composites were tested for compressive strength to identify their mechanical properties, and an acid attack durability test exposed to 3.5% sulfuric acid solution to identify their corrosion performance in an aggressive acid environment. X-ray diffraction, thermogravimetric and scanning electron microscopic analysis were carried out to ascertain the physicochemical properties of the cement composites. The results show that an eco-friendly zero cement concrete developed with a quaternary blended mix of nano-silica, fly-ash, slag and hydrated lime successfully addresses the mechanical and durability requirements of the concrete sewage pipes. It surpasses ASTM's minimum strength requirement for the sewage pipes, and brings about a significant improvement in withstanding an aggressive acidic environment as evident from the 96% reduction in its mass loss due to concrete corrosion, compared to that of the OPC concrete. Moreover, the high amorphous silica content present in nano silica, slag and fly-ash assists in totally consuming the free lime that interacts with fat, oil and grease to produce fatbergs.

1. Introduction

Climate change brought about by greenhouse gas emissions is a significant challenge facing our planet [Bongaarts, 2019]. The cement and concrete industry is one of the major producers of greenhouse gases that accounts for about 5% of the total global greenhouse gas emissions [Andrew, 2018]. Therefore, it has been designated as an essential research area for a long time. Various advancements have been made in the use of alternative materials, processes and technologies to reduce its carbon footprint and to improve the energy efficiency of cement production [Zuberi and Patel, 2017, Talaei et al., 2019]. Some of the factors adopted by the cement industry are, use of alternative fuels [Georgiopoulou and Lyberatos, 2018, Chatziaras et al., 2016], blending cement with various industrial by-products like fly-ash [Roychand et al., 2016, Roychand et al., 2016, Roychand et al., 2017, Roychand, 2017] slag [Roychand, 2017, Roychand et al., 2018, Jiang et al., 2018] and silica fume [Roychand et al., 2016, Pedro et al., 2017] and replacement of conventional aggregates with different industrial waste products like bottom ash [Singh et al., 2018], granular slag [Roychand et al., 2020], crushed glass [Islam et al., 2017, Lalitha et al., 2017, Saberian et al., 2019], recycled aggregates [Saberian et al., 2020] and waste tyre rubber [Saberian and Li, 2018, Youssf et al., 2019, Abd-Elaal et al., 2019, Roychand et al., 2020]. Although a large number of industrial [Hilton et al., 2019], agricultural [Madandoust et al., 2011, Aprianti et al., 2015, Debbarma et al., 2020] and municipal waste materials [Ashraf et al., 2019] have shown potential to be used as supplementary cementitious materials (SCM), they require extensive long-term studies before being accepted by the construction industry. Therefore, fly ash, slag and silica fume are by far the most widely used SCM to date. With the advancement in research, the

* Corresponding author.
E-mail address: rajeev.roychand@rmit.edu.au (R. Roychand).

https://doi.org/10.1016/j.resconrec.2020.105166
Received 8 June 2020; Received in revised form 10 September 2020; Accepted 13 September 2020

share of blended cement in the total quantity of cement manufactured has significantly increased over time, due to its growing acceptance by the construction industry and the emerging awareness about the importance of green environment [Sar, 2018.

It is well established that SCM play a vital role in improving the durability properties of concrete [Juenger and Siddique, 2015, Gedam et al., 2016]. Though ordinary Portland cement (OPC) is the most widely used cementitious material in the fast-paced construction industry, it poses long term durability issues in some of the applications [Bastidas-Arteaga and Schoefs, 2015, Alexander, 2016]. One of the major such applications is prefabricated concrete sewage pipes that act as the backbone of the sanitation system. The various issues that plague these concrete structures are corrosion of concrete [Wasim et al., 2020, Wasim and Hussain, 2015] due to the acidic environment produced by the microbial activity within the sewage water [Mori et al., 1992, Mori et al., 1991, Wells et al., 2009, Wu et al., 2018] and the clogging of these pipes due to fat, oil and grease (FOG) accumulation [Oakes, 2019, Wallace et al., 2017]. Microbiologically induced concrete corrosion (MICC) [Wasim and Djukic, 2020] of sewage pipes can lead to the leaching of significant amounts of calcium, OH^- and SO_4^{2-} ions [Hermansyah et al., 2006]. Previous research studies show that high concentrations of calcium salts play an important role in the deposition and accumulation of FOG within the drainage pipes, eventually clogging the drainage system [Oakes, 2019, Wallace et al., 2017, He et al., 2013, Keener et al., 2008]. This shows that the free lime present in ordinary Portland cement concrete plays a detrimental role in (i) corroding the sewage pipes when exposed to the microbe induced acid environment and (ii) leaching of lime from concrete that interacts with FOG to produce Farbergs (calcified form of FOG), thereby clogging the sewage network (Fig. 1).

Maintaining and upgrading the sewage network comes with high costs and disruptions to the general public. Water Services Association of Australia estimates the cost of maintenance of sewage networks to be about $15 million each year [46], which costs about $25 billion in the USA and £15–50 million in the United Kingdom [Williams et al., 2012, Del Mundo and Sutheerawattananonda, 2017]. Considering the huge cost associated with the maintenance of sewage drainage network, it is imperative to look for long term sustainable solutions for issues plaguing the sewage drainage network.

Previous studies show that the addition of fly-ash [Aydın et al., 2007, Torii and Kawamura, 1994, Jeon et al., 2006], slag [Jeon et al., 2006], silica fume [Torii and Kawamura, 1994, Jeon et al., 2006], and nano-silica [Mahdikhani et al., 2018, Deb et al., 2016] improve the acid resistance of blended concrete mixes by consuming free lime released by the hydration reaction of OPC. Another study by Kusum et al. [Kusum et al., 2018] showed positive benefits of using alternative binder materials for sewer concrete structures to reduce fat, oil, and grease related sanitary sewer overflows. All these SCM at different replacement levels [Aydın et al., 2007, Jeon et al., 2006, Kusum et al., 2018, Xie et al., 2018, Li and Peethamparan, 2018] have shown positive benefits in addressing these issues. However, based on the authors best knowledge, there is very limited or no research available on the development of an eco-friendly zero cement composite that can withstand the acidic environment present within the sewage pipes and can eliminate the residual lime that leaches out and contributes towards the formation of fatbergs, thereby clogging the sewage pipes. Therefore, to address this research gap, an experimental investigation was undertaken in a progressive stepped approach replacing 70 – 100% of OPC to develop a zero cement concrete that meets the strength requirements of concrete sewage pipes [ASTM International. C76M-19b 2019] and can withstand the aggressive acid environment present in the sewage water. In addition, this study aims to minimise or eliminate the free lime content present in hardened cement concrete that can potentially leach out and interact with FOG resulting in the deposition and accumulation of its calcified form thereby clogging the sewage pipes.

2. Materials and methodology

2.1. Materials

The materials used in this research were; OPC, ground granulated blast furnace slag (Slag), fly-ash (FA) and hydrated lime (HL) sourced from Cement Australia P/L, nano-silica (NS) sourced from Sigma Aldrich P/L and superplasticizer “Master Glenium SKY 8379” sourced from BASF Australia P/L.

2.2. Methodology

The experimental program was carried out in a two staged process. In the first stage, the physical, chemical, and mineralogical properties of the raw material were investigated i.e. ordinary Portland cement, slag, fly-ash and nano-silica using laser diffraction particle size analysis, X-ray fluorescence (XRF) and X-ray diffraction (XRD). In the second stage, the compressive strength of the different concrete mixes and their performance in an aggressive acidic environment were studied. The 28-day cured hardened concrete samples were soaked in 3.5% sulfuric acid solution, having a pH value of 0.2, for 28 and 56 days. A study conducted by Vincke et al. [Vincke et al., 2001] on the acidic environment of the corroded sewage pipes found that their pH varied between 7.2 (neutral) in the biofilm covering the bottom and 2.9 (acidic) at the crown of the sewer pipe. The corrosion of the concrete pipes under this level of acidic pH progresses slowly and is a long-term process.

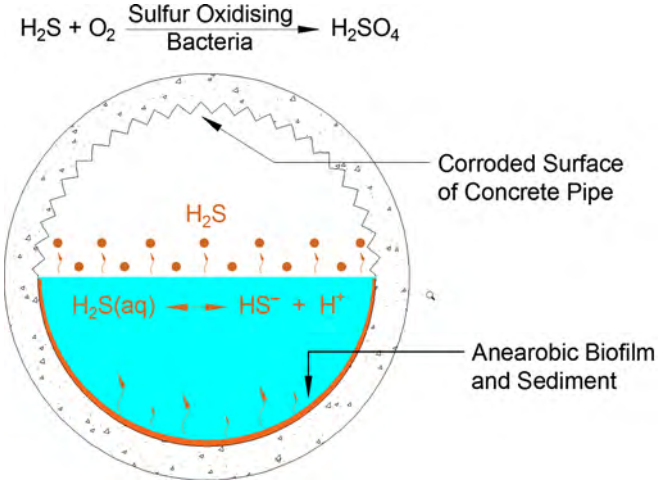

Fig. 1. Acid corrosion and FOG clogging of concrete pipes (recreated from the original sources [Wu et al., 2018, FOG, 2018])

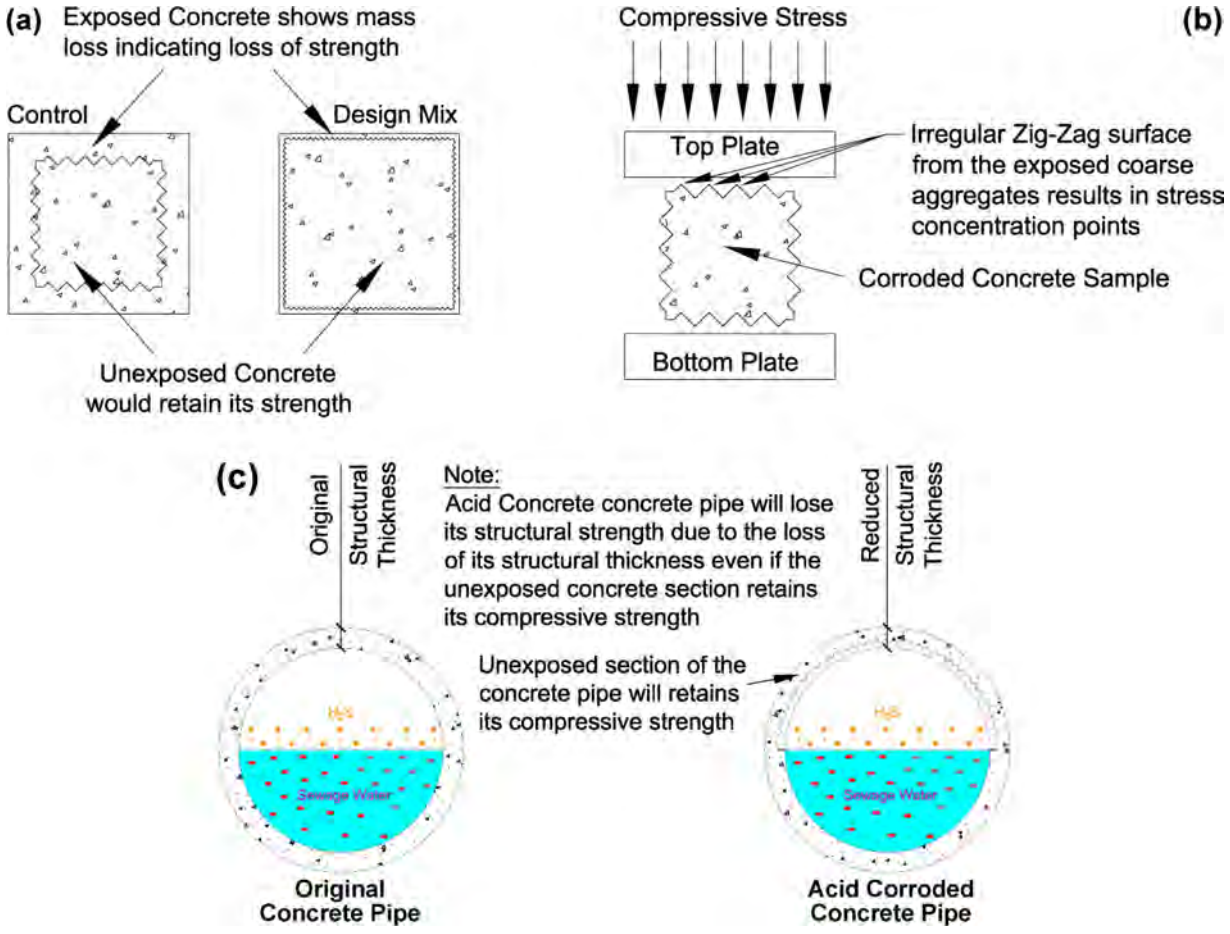

Fig. 2. Relevance of compressive strength test on acid corroded samples

Therefore, to address the time constraints, this experiment was carried out in an aggressive accelerated environment by using very low (0.2) pH 3.5% sulfuric acid solution. To identify the effect of the aggressive acid environment on concrete corrosion a range of concrete mixes were assessed for mass loss after 28 and 56 day soaking in the acid solution. Photographic images were also taken for visual identification of the corroded state of the concrete cubes of the different mix designs. Ideally compressive strength tests could be carried out to ascertain the reduction in the compressive strength of the acid corroded concrete in comparison to the original sample (the ones not kept in acid solution). However, there are various factors that affect the compressive strength results of the acid corroded samples, as discussed below:

The compressive strength of the concrete would vary between the sections exposed and unexposed to the acid environment. Moreover, the deterioration of concrete is not consistent among all the samples with very irregular and zig-zag surface. A lot of approximation in the measurement of the dimensions would be required to measure force/stress-area to ascertain the compressive strength, that may not be a true reflection of the actual compressive strength of the corroded sample (Fig. 2(a)).

The corroded concrete has irregular zig-zag shape with exposed coarse aggregates and carrying out compressive strength test on such a sample would have stress concentration points as shown in Fig. 2(b). Therefore, the compressive strength of the tested sample would not be reflective of their true values.

The structural strength of a concrete pipe would be affected by the reduction in the structural thickness (i.e. mass loss due to corrosion). Even if the unexposed section of the concrete pipe or any structural member in general has no loss of compressive strength, the structural member would still lose its design structural strength because of the reduction in its profile thickness (i.e. again can be represented with the mass loss of concrete). Please refer Fig. 2(c) for further details.

To ascertain the physicochemical changes taking place within the cement matrix due to the variation in the mix designs, and their effect on the concrete corrosion, XRD and TGA analysis were carried out on the hardened cement paste samples and SEM on hardened concrete samples.

2.2.1. Chemical and mineral composition of ordinary portland cement, slag, fly-ash and nano silica

The chemical composition of ordinary portland cement, slag, fly-ash, and nano-silica were obtained using Bruker AXS S4 Pioneer X-ray fluorescence instrument. Table 1 shows the chemical composition of the OPC, slag, fly ash, and nano-silica.

X-ray diffraction (XRD) was conducted on oven-dried powder samples of ordinary portland cement, slag, fly-ash and nano silica (Fig. 3) using the following equipment and settings:

XRD equipment: Bruker AXS D4 Endeavour
Detector: lynxeye linear strip detector
X-ray radiation source: Cu-Kα
Current and voltage settings: 40-mA current and 40-kV voltage

Table 1
Chemical composition

Materials	SiO_2	CaO	Al_2O_3	Fe_2O_3	SO_3	MgO	Na_2O	K_2O	TiO_2
OPC	21.8%	63.9%	5.1%	3.8%	2.2%	2.4%	0.3%	0.2%	0.3%
Slag	30.3%	47.8%	12.9%	0.4%	2.7%	4.5%	0.4%	0.5%	0.5%
FA	73.5%	0.4%	22.5%	1.1%	0.2%	0.4%	0.2%	0.3%	1.4%
NS	99.9%	-	-	-	-	-	-	-	-

Table 2
Amorphous and crystalline composition of OPC and Slag

	C_2S	C_3S	C_4AF	C_3A	CC	MgO	$C\bar{S}(G)$	CH	$C\bar{S}(B)$	Quartz	Amorphous
OPC	6.7%	63.4%	7.1%	7.4%	7.2%	2.2	3.6%	1.2%	0.9%	0.3	-
Slag	2.9%	-	-	-	2.7%	-	4.7%	-	-	-	89.7%

$C_3S = Ca_3SiO_5$, $C_2S = Ca_2SiO_4$, $C_3A = Ca_3Al_2O_6$, $C_4AF = Ca_2Al_{0.37}Fe_{1.63}O_5$, $CH = Ca(OH)_2$, $C\bar{S}(G) = CaSO_4.2H_2O$), $CC = CaCO_3$, $C\bar{S}(B) = CaSO_4.0{\bullet}5H_2O$

Table 3
Amorphous and crystalline composition of fly ash

Material	Crystalline phases				Amorphous phases	
	SiO_2	$Al_{4.6}Si_{1.4}O_{9.7}$	Fe_3O_4	TiO_2	SiO_2	Al_2O_3
Fly ash	23.7%	29.2%	1.3%	1.1%	43.7%	1.0%

Table 4
Particle size distribution in microns (μm)

Particle Size	OPC	Fly ash	Slag	Nano silica*
D_{10}	2.7	2.2	2.7	7 nm
D_{25}	6.5	5.7	6.6	-
D_{50}	15.4	13.9	14.1	-
D_{75}	28.3	32.9	23.6	-
D_{90}	44.2	75.1	33.6	-
D[4,3] Mean	24.6	28.6	16.4	-

* Particle size in nanometers

Testing range: 5° to 70° 2-theta
Step size: 0.01° 2-theta
Counting time: 1 s per step.

2.2.2. Concrete mix designs

Table 5 shows all the mix designs investigated in this study. Hydrated lime was used as an alkaline activator in the mix designs not containing any OPC content. The various combinations of cementitious material (i.e. OPC, slag, fly ash, and nano silica) and hydrated lime were selected based on our previous studies [Roychand et al., 2016, Roychand et al., 2016, Roychand et al., 2017, Roychand et al., 2018]. Water cement ratio was kept low to reduce concrete porosity which is beneficial with regard to the durability properties of the concrete mixes [Kim et al., 2014]. Superplasticizer was added to all mix designs to assist in reducing the w/c and separation of the individual particles of the cementitious material [Nkinamubanzi et al., 2016], which further improves the hydration/pozzolanic reaction of the cement composites. The quantity was varied based on trial mixes to achieve similar consistency of the wet mixes. Since nano-silica has very high surface area it significantly increases the superplasticizer requirement [Sonebi et al., 2015].

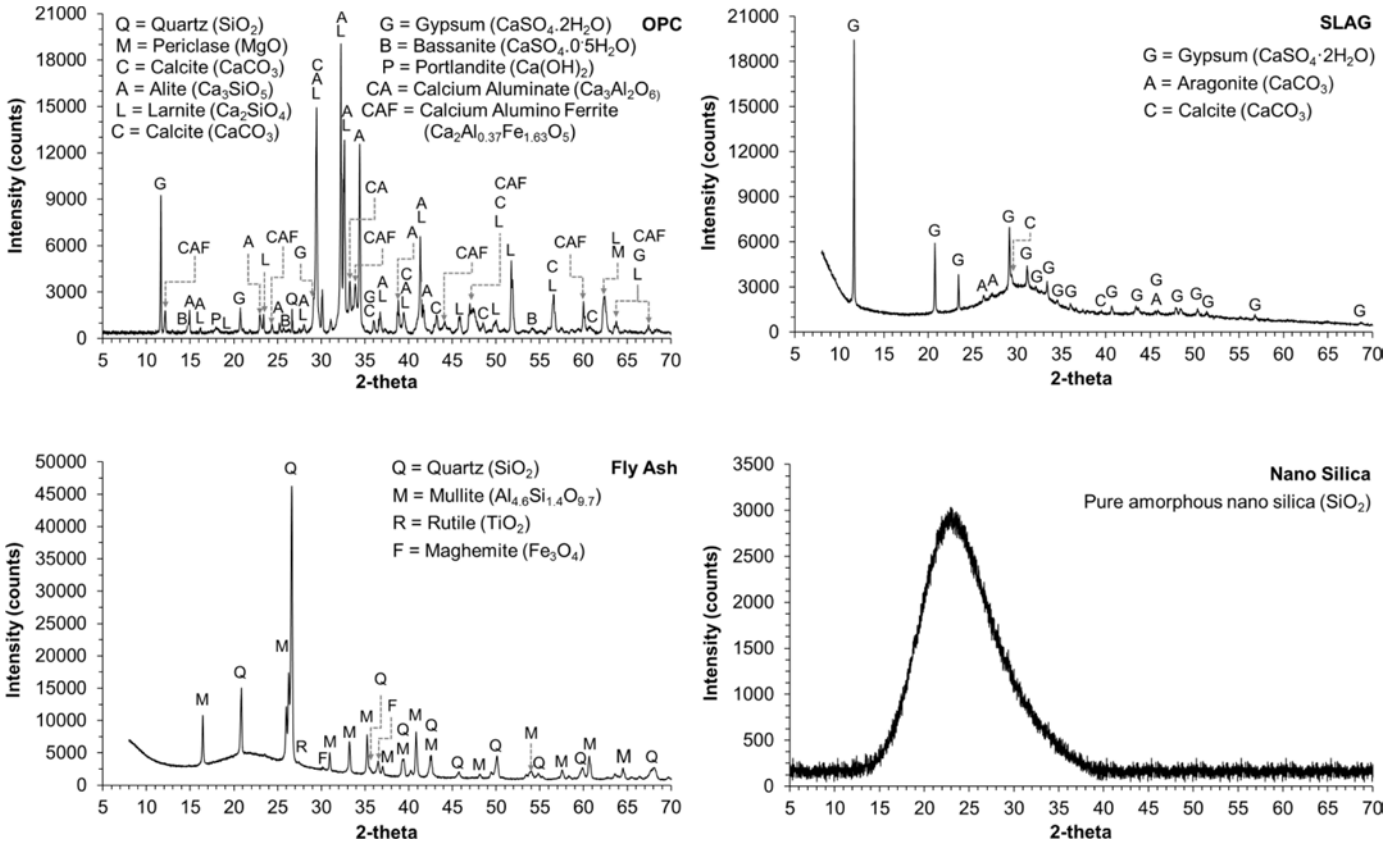

Fig. 3. X-ray diffractograms of OPC, Slag, fly ash and nano silica the amorphous and crystalline mineral composition of OPC and slag are presented in Table 2 and that of fly-ash are shown in Table 3. The particle size distribution of the raw powdered binder material is presented in Table 4.

Table 5
Concrete mix design

Design Mix	Percentage Cementitious material (CM)				HL (% of CM)	S/CM (by weight)	CA/CM (by weight)		W/CM	SP
	OPC	Slag	FA	NS		< 2.36mm	7mm	14mm		
C	100	-	-	-	0	1.5	1.15	1.1	0.3	12
M 1	25	-	75	-	0	1.5	1.15	1.1	0.3	10
M 2	25	-	70	5	0	1.5	1.15	1.1	0.3	45
M 3	-	25	75	-	15	1.5	1.15	1.1	0.3	20
M 4	-	25	70	5	15	1.5	1.15	1.1	0.3	55
M 5	30	-	70	-	0	1.5	1.15	1.1	0.3	10
M 6	30	-	65	-	0	1.5	1.15	1.1	0.3	45
M 7	-	30	70	-	15	1.5	1.15	1.1	0.3	20
M 8	-	30	65	5	15	1.5	1.15	1.1	0.3	55

S = sand, CA = coarse aggregate, W = water, SP = superplasticizer (mLkg^{-1} of cementitious material)

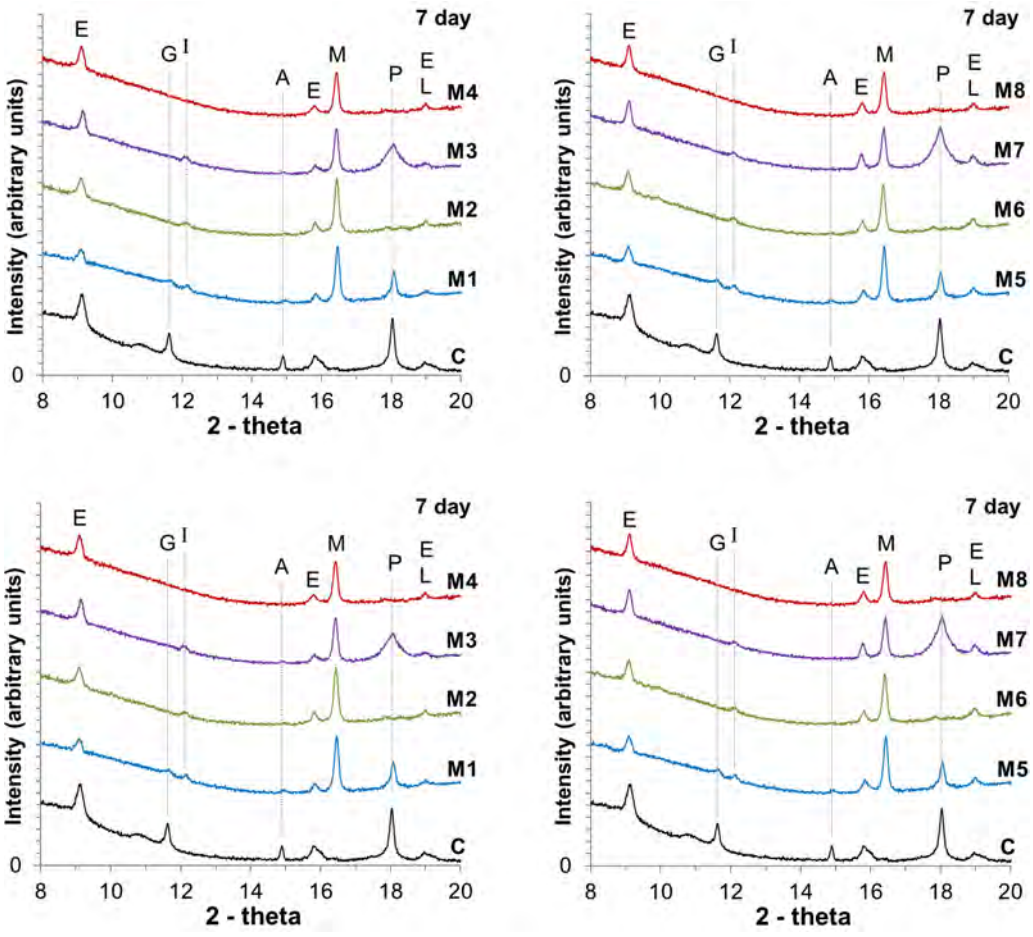

Fig. 4. XRD diffractograms of hydrated cement paste samples at 7 and 28 days of curing

2.2.3. Experimental program

2.2.3.1. Concrete compressive strength. Three replicates of 100Ø x 200mm concrete cylinders were cast for concrete compressive strength test for 7, 28 and 56 days of curing age. All the samples were cured as per AS 1012.8.1: 2014 [AS 1012.8.1 2014] and tested at 7, 28 and 56 in accordance with AS 1012.9:2014 [AS 1012.9:2014 2001].

2.2.3.2. XRD and TGA of hydrated paste. 25mm cube cement paste samples were casted for X-ray diffraction and thermogravimetric analysis, keeping the same curing conditions as that of the concrete samples. One day before the day of testing the hardened cement paste samples were taken out of the curing water and air dried for 24 hrs. On the day of testing they were finely crushed using pestle and mortar. Unreacted physically bound water present in the crushed material was removed using solvent replacement method as described in [Roychand et al., 2017]. The solid material was filtered out from the solvent, dried for 24 hours in an oven at 45 degree centigrade temperature, micronized using a ring mill and kept in sealed plastic containers before carrying out X-ray diffraction (XRD) and thermogravimetric analysis (TGA). Quartz present as a crystalline component of fly ash shows very strong peaks and it suppresses other important peaks of ettringite, portlandite and gypsum, therefore the XRD data was conducted on the dried and micronized cement paste samples from 5° to 20° 2-theta using the same instrument settings as described in Section 2.2. The XRD data was analysed in conjunction with the TGA

data to get a clear understanding of chemical changes taking place within the hardened cement paste of various mix designs.

TGA was carried out using PerkinElmer STA 6000 equipment in an inert environment using nitrogen. The flow rate of nitrogen was maintained at 19.8mL min^{-1}. The dried cement paste samples were tested between 40 and 850 °C temperature with a heating rate of 20 °C min^{-1}.

2.2.3.3. SEM of 28 day cured hydrated concrete. The scanning electron microscopy (SEM) was carried out on a small section taken out from the internal part of the concrete sample using FEI Quanta 200 SEM at magnification level of 2500x.

2.2.3.4. Concrete acid attack (Sulphuric acid). 100 × 100 × 100mm concrete cube samples were initially cured for 27 days, dried in a convection oven at 30 °C for one day, weighed for their initial dry mass and then dipped in 3.5% Sulfuric acid solution having a pH value of 0.2, for another 28 and 56 days. The pH of the acid solution was checked every week and maintained at the same pH value. On the day of testing, the samples were taken out of the acid solution washed with plain water to remove any loose material, dried in a convection oven at 30 °C for one day and then weighed to check for any mass loss. Low-temperature drying was undertaken to preserve various phases, like C-S-H/C-A-S-H, Aft and AFm, that have low thermal breakdown temperatures varying between 50 – 250 °C [Scrivener et al., 2016].

3. Results and discussion

3.1. X-ray diffraction and thermogravimetric analysis

Fig. 4 shows X-ray diffractograms of hydrated cement pastes of various mix designs at 7 and 28 days of curing. Since quartz present in fly-ash shows a very strong XRD peak that overshadows the other smaller but important peaks such as ettringite, gypsum, and portlandite etc., the XRD data is presented from 5 to 20 °2θ. The various phases identified in the XRD diffractograms were E = ettringite [Ca_6 $Al_2(SO_4)_3$ $(OH)_{12}$ • $26H_2O$], G = gypsum [$CaSO_4$ • $2H_2O$], I = ilvaite [$CaFe_3Si_2O_8(OH)$], A = Alite [Ca_3SiO_5], M = mullite [$Al_{2.28}O_{4.86}Si_{0.72}$], P = portlandite [$Ca(OH)_2$], L = larnite [$Ca_2SiO_4$]. The results are discussed in detail in Section 3.3 compressive strength analysis.

Fig. 5 shows the derivative curves of the TGA data of all mix designs at 7 and 28 days of curing. To reduce the noise in the derivative curves the data was smoothened using origin software. The TGA data is analysed in detail in Table 6. The second column shows the actual mass loss from overlapping group of phases i.e. C-S-H/C-A-S-H/AFt/AFm, and gypsum (where present). The third column shows the ideal mass loss of the same group of phases based on the hydration reaction of the actual amount of OPC present in the mix design, assuming if no pozzolanic reaction takes place. To explain further, mass loss of 100% OPC mix, between 50 – 250 °C temperature at 7 days of curing = 7.18% (Table 6)

Therefore, the ideal mass loss of a blended mix containing 25% OPC (M1) at the same temperature range and curing age should have been = $\frac{25}{100}$ x 7.18% = 1.8% (rounded off)

Similar way the calculations for C-A-H were performed. CH_i (portlandite) and CC_i (calcite) as shown in columns 6 and 7 in Table 6 are the actual amounts of these phases identified through the TGA analysis at particular curing ages. The identified CH_i and CC_i were calculated from the mass loss due to the release of chemically bound H_2O and CO_2 from portlandite and calcite are as shown below:

$$CH_i = \frac{M_{H2O\ CH} * \frac{74}{18}}{M_{50}} * 100\ [\%] \quad \text{(E1)}$$

$$Ca(OH)2 \xrightarrow{\sim 390-510^{\circ}C} CaO + H2O \uparrow \quad \text{(R1)}$$

$$CC_i = \frac{M_{CO2\ CC} * \frac{100}{44}}{M_{50}} * 100\ [\%] \quad \text{(E2)}$$

$$CaCO3 \xrightarrow{\sim 510-800^{\circ}C} CaO + CO2 \uparrow \quad \text{(R2)}$$

Equation (E1) provides the formula to calculate the actual quantity of $Ca(OH)_2$ present in the hydrated cement paste using the TGA analysis. The mass loss of the chemically bound water due to the thermal

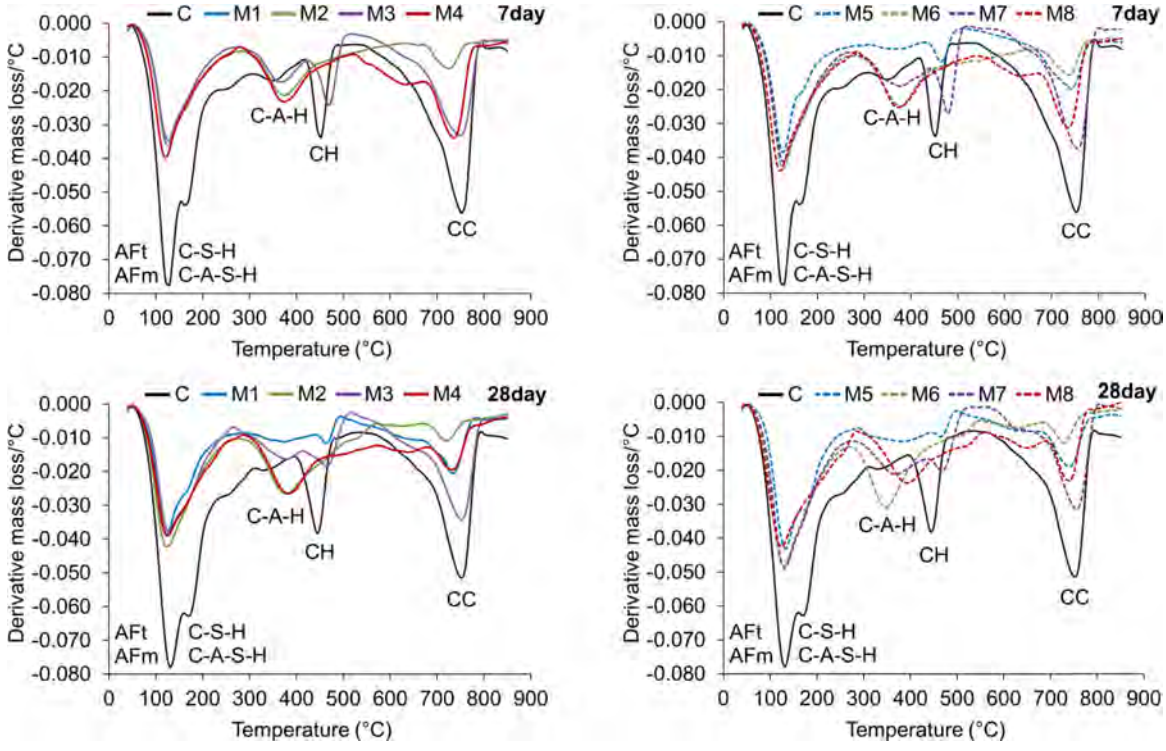

Fig. 5. Derivative thermogravimetric curves of hydrated cement paste samples

Table 6
TGA data analysis - mass loss due to the thermal breakdown of different phases/group of phases

Mix	C-S-H/C-A-S-H / Aft / AFm / Gypsumchemically bound water (%)				C-A-Hchemically bound water (%%				Identified CH_i (%)		Identified CC_i (%)		Actual Released CH_{ar} (%)		Ideal Release CH_{ir} (%)	
	Actual Formation		Ideal Formation		Actual Formation		Ideal Formation									
	7d	28d	7d	28d	7d	28d	7d	28d	7d	28d	7d	28d	7d	28d	7d	28d
C	7.18	8.56	7.18	8.56	1.30	1.37	1.30	1.37	4.60	7.08	12.01	10.90	13.49	15.15	13.49	15.15
M 1	2.28	3.13	1.80	2.14	0.62	0.90	0.33	0.34	1.31	1.02	3.12	3.91	3.62	3.91	3.37	3.79
M 2	3.30	4.18	1.80	2.14	3.24	3.94	0.33	0.34	-	-	2.05	2.30	1.52	1.70	3.37	3.79
M 3	3.07	3.54	0.00	0.00	1.54	1.87	0.00	0.00	4.51	4.36	7.90	6.33	10.36	9.04	13.04	13.04
M 4	3.44	4.31	0.00	0.00	2.83	3.25	0.00	0.00	-	-	9.20	6.19	6.81	4.58	13.04	13.04
M 5	2.98	4.12	2.15	2.57	0.66	1.38	0.39	0.41	1.50	1.31	4.20	5.05	4.61	5.05	4.05	4.55
M 6	4.07	4.95	2.15	2.57	3.57	4.07	0.39	0.41	-	-	2.43	2.67	1.80	1.98	4.05	4.55
M 7	3.73	4.34	0.00	0.00	2.21	2.41	0.00	0.00	4.37	3.95	6.67	5.69	9.31	8.16	13.04	13.04
M 8	4.17	4.86	0.00	0.00	3.31	3.67	0.00	0.00	-	-	7.87	5.48	5.82	4.06	13.04	13.04

breakdown of $Ca(OH)_2$ as per reaction (R1) is used to calculate the original mass of $Ca(OH)_2$ present in the sample. Equation (E2) provides the formula to calculate the actual amount of $CaCO_3$ present in the hydrated cement paste. The mass loss of the chemically bound CO_2 due to the thermal breakdown of $CaCO_3$ as per reaction (R2) is used to calculate the original mass of $CaCO_3$ present in the sample.

Where, $M_{H2O\,CH}$ = mass loss from dehydroxylation of portlandite

Fraction $\frac{74}{18}$ to convert $Ca(OH)_2$ bound water into actual $Ca(OH)_2$ mass

Molar mass of $Ca(OH)_2$ = 74 and that of H_2O = 18.

$M_{CO2\,CC}$ = mass loss from the de-carbonation of the $CaCO_3$

Fraction $\frac{100}{44}$ to convert mass loss due to CO_2 to $CaCO_3$ mass

Molar mass of $CaCO_3$ = 100 and that of CO_2 = 44

It is to be noted that part of the portlandite gets converted to calcite on coming in contact with carbon dioxide present in the atmosphere. Therefore, to identify the actual portlandite released by the hydration reaction of calcium silicates (C_2S and C_3S) present in OPC, the identified CC_i (calcite) was converted into its portlandite equivalent using the following formulae:

$$\text{CaO mass} = \frac{\text{CaCO3 mass}}{100}\ x\ 56\ \text{[To convert CaCO3 into CaO]} \quad \text{(E3)}$$

$$\text{Ca(OH)2 mass} = \frac{\text{CaO mass}}{56}\ x\ 74\ \text{[To convert CaO into Ca(OH)2]} \quad \text{(E4)}$$

Equation (E3) provides the formula to calculate the amount of CaO present in the identified $CaCO_3$ that is further used to calculate the total $Ca(OH)_2$ as per equation (E4), that ideally would have been present if none of it had been converted into $CaCO_3$ on coming in contact with the atmospheric CO2.

In equations (E3) and (E4), 56 is the molar mass of CaO, 100 is of $CaCO_3$ and 74 is of $Ca(OH)_2$. The portlandite equivalent obtained from the conversion of calcite is added to the portlandite identified in the TGA analysis to obtain the total portlandite released by the hydration reaction of calcium silicate (C_2S and C_3S) phases and is termed as CH_{ar} as shown in column 8 of Table 6. Column 9 shows the portlandite content that should have ideally been released by the hydration reaction of the actual percentage of OPC present in a particular mix design. The results are discussed in detail in section 3.3 compressive strength analysis.

3.2. Scanning electron microscopic analysis

Fig. 6 shows the microscopic images of the hardened concrete samples at 28 days of curing. The control mix containing 100% OPC shows a very dense matrix along with shrinkage cracks. On partially replacing OPC with 75% fly ash in M1, a significant reduction in the strength forming gel formation along with a large number of unreacted fly ash particles were observed in the cement microstructure. With the increase in the cement content from 25% in M1 to 30% in M5 followed by the corresponding reduction in the fly ash content from 70% to 70%, an increase in the gel formation and the reduction in the unreacted fly ash particles were observed.

In M2, the fly ash content was partially replaced with 5% nano silica, which brought about a considerable increase in the gel formation followed by a considerable reduction in unreacted fly ash particles indicating that nano silica not only increases the strength forming gel it also accelerated the pozzolanic reaction. With a further increase in the OPC content from 25% in M2 to 30% in M6, followed by the reduction in the corresponding fly ash content from 70% to 65% and keeping the nano silica content as 5%, an improvement in the gel formation followed by the refinement of the microcracking was observed. In M3 the 25% OPC component of M1 was replaced with 25% of slag, together with 15% addition of hydrated lime as an alkaline activator. The SEM image of M3 showed a similar microstructure to that of M1. However, the strength forming gel in case of M1 was produced by the hydration reaction of OPC and the pozzolanic activity of fly ash, but in case of M3 the whole strength forming gel was produced by the pozzolanic activity of fly ash and slag. With a further increase in the slag content from 25% in M3 to 30% in M7, followed by a reduction in the corresponding fly ash content from 75% to 70% an improvement in the gel formation was observed in comparison to that of M3. In M4, the fly ash content of M3 was partially replaced with 5% nano silica. This replacement brought about a considerable increase in the gel formation followed by a considerable reduction in the unreacted fly ash particles again reinforcing our earlier observation that nano silica not only increases the strength forming gel it also accelerates the pozzolanic reaction of the cement composites. On increasing the slag component from 25% in M4 to 30% in M8 followed by the corresponding reduction in the fly ash content, the SEM image of M8 did not show any significant difference in the cement microstructure to that of mix M4. However, a noticeable increase in the strength forming gel was identified in nano silica modified mix M8 in comparison to that of mix M7 not comprising nano silica.

3.3. Compressive strength analysis

Fig. 7 shows the compressive strength results of the concrete samples at 7, 28 and 56 days of curing. By replacing 75% of OPC with flyash in M1 there was 75.8, 63.3 and 56% reduction in the 7, 28 and 56 day compressive strength results compared to that of the control mix. The reduction in the compressive strength with the addition of fly ash has also been reported by other researchers [Şahmaran et al., 2009, Liu, 2010]. This was also reflected in a significant reduction in the mass loss between 50 to ~250 °C temperature (Table 6) that includes the major strength forming C-S-H/C-A-S-H phases including the ettringite phase that also contributes towards the initial strength [Midgley and Pettifer, 1971, Yan et al., 1999].The ideal release of portlandite from the reaction of calcium silicate phases was 3.37% and 3.79% at 7 and

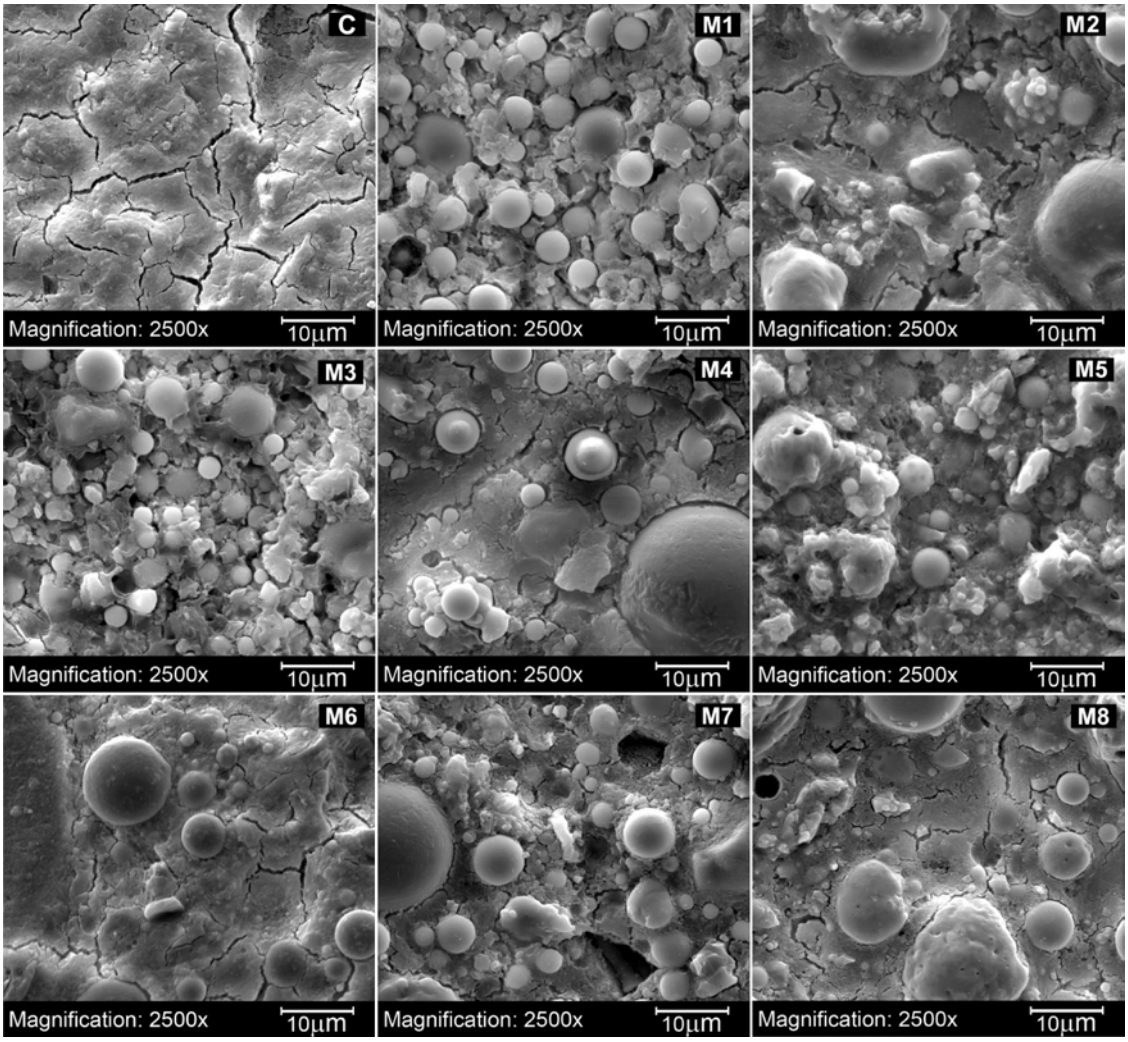

Fig. 6. SEM images of concrete samples at 28 days of curing

28 days, respectively; however the actual release was higher i.e. 3.62% and 3.79%. Corroborating the ideal vs actual portlandite release with ideal vs actual formation of C-S-H/C-A-S-H/C-A-H phases, it was noticed that the actual C-S-H/C-A-S-H/C-A-H phases recorded were more than what ideally should have formed by the hydration reaction of 25% OPC content in M1. This indicates that the actual release of portlandite was more than the resultant recorded in the 7 and 28 days showing the increase in the hydration reaction of OPC, a part of which reacted with

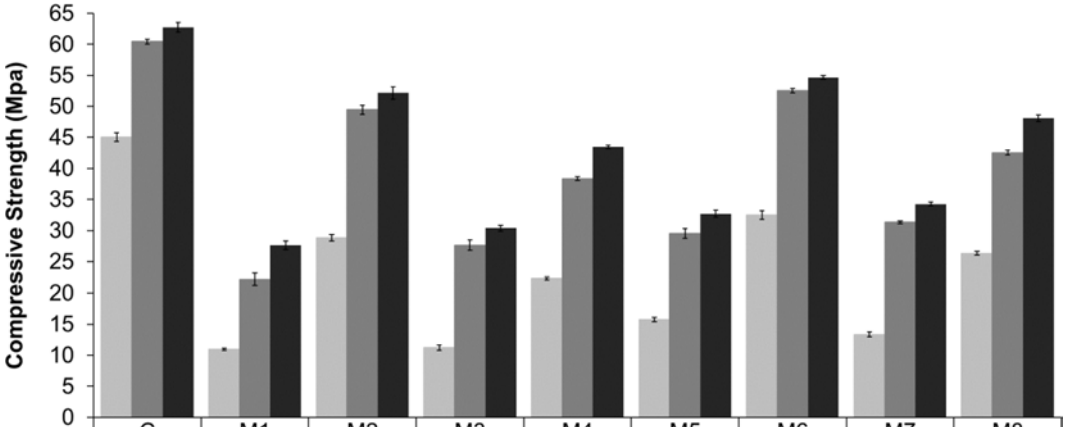

	C	M1	M2	M3	M4	M5	M6	M7	M8
7 day	45.0	10.9	28.8	11.2	22.4	15.8	32.5	13.3	26.3
28day	60.4	22.2	49.4	27.6	38.4	29.5	52.6	31.3	42.5
56day	62.7	27.6	52.1	30.4	43.5	32.7	54.6	34.2	48.1

Fig. 7. Concrete compressive strength results

fly-ash to produce additional C-S-H/C-A-S-H/C-A-H content. The SEM images of M1 show a large number of unreacted and partly reacted fly-ash particles with the sparse formation of the strength forming gel compared to the dense matrix of the control mix providing the micro-structural evidence of the reduction in strength of M1 compared to that of the control mix.

When the OPC content was increased in mix M5, there was 45, 32.9, 18.5% improvement in the respective 7, 28 and 56 day compressive strength results, in comparison to that of mix M1. The increase in strength was clearly reflected in the corresponding increase in the C-S-H/C-A-S-H and C-A-H gel formations in addition to the increase in the actual portlandite released (CH_{ar}) within the cement matrix of M5, in comparison to that of M1 (Table 6). This also shows an improvement in the hydration/pozzolanic reaction because of the increase in OPC content and the decrease in the fly-ash content. The increased amount of OPC produces higher C-S-H/C-A-S-H and C-A-H gel in addition to the increased release of portlandite content that is exposed to the higher amount of fly-ash particles thereby increasing the pozzolanic reaction and producing additional strength imparting C-S-H/C-A-S-H/C-A-H gel. This increased gel formation was also reflected in the SEM image of M5 compared to that of M1 (Fig. 6).

In mix M2 a part of the fly-ash content of M1 was replaced with 5% of amorphous nano-silica, keeping the remaining material composition the same as that of M1. With the replacement of a part of fly-ash with nano-silica, M2 showed 164.2, 122.5 and 88.8% improvement in its compressive strength results, which was also reflected in the increase in the C-S-H/C-A-S-H and C-A-H content followed by the total consumption of the portlandite released by the hydration reaction of OPC. The positive effect of the increase in compressive strength with the addition of nano silica has been reported by other researchers [Zhang and Islam, 2012, Hou et al., 2013]. The increase in C-S-H content followed by the total consumption of portlandite clearly shows the increased pozzolanic reaction of nano-silica that contributed towards its strength improvement [Roychand et al., 2018]. However, a significant increase in the C-A-H (Table 6) and ettringite contents (Fig. 4) of M2 compared to that of M1 indicate that the addition of nano-silica not only increases the pozzolanic reaction it also accelerates the hydration/pozzolanic reaction of the blended cement composites [Roychand et al., 2018, Björnström et al., 2004]. The SEM image of M2 shows a significant increase in its strength forming gel, indicating a substantial improvement in its cement microstructure, compared to that of M1. On increasing the OPC content to 30% in mix M6, it showed 12.9, 6.5, 4.8% improvement in corresponding compressive strength results at 7, 28 and 56-days of curing, in comparison to that of mix M2. This was supported by the increase in C-S-H/C-A-S-H and C-A-H contents followed by the total consumption of the portlandite which ideally must have been released in higher quantity than that of mix M2 because of the increase in OPC content. There was a small increase in the ettringite peak of M6 compared to that of M2 as seen in the XRD diffractograms because of the increase in sulfate and calcium aluminate contents from the increased percentage of OPC in M6. The increase in the C-S-H/C-A-S-H and C-A-H contents followed by the increase in compressive strengths of M6 compared to that of M2 were also supported by the denser microstructure with finer microcracks in M6 compared to that of M2. Similar observations were reported by other researchers in previous studies [Singh et al., 2013, Zhang et al., 2018].

Mix M3 had a similar mix design as that of M1 but the OPC content present in M1 was replaced with slag in M3. Both slag and fly-ash need alkaline activator for the pozzolanic reaction therefore hydrated lime was added to the mix design as an alkaline activator. At 7 days M3 showed similar strength as that of mix M1, however at the curing ages of 28 and 56 days, it showed 24.3 and 10.1% improvement in compressive strength compared to that of M1. Even though there was no noticeable change between M3 and M1 compressive strengths at 7 days, M3 showed higher mass loss associated with the C-S-H/C-A-S-H/AFt/AFm group of phases than that of M1. This increase in mass loss is most likely due to an increase in ettringite content of M3 compared to that of M1, which contains a considerably higher amount of chemically bound water compared to that of the C-S-H/C-A-S-H phases. The increase in C-S-H/C-A-S-H and C-A-H phases followed by a considerable consumption of portlandite content as can be seen in CH_{ar} vs CH_{ir} contents clearly indicating the pozzolanic reactivity of amorphous silica and alumino-silicates phases present in slag and fly-ash, that contributed towards the strength development of M3 at various curing ages. The SEM image of M3 shows a similar microstructure to that of M1. The only difference is the strength forming gel in case of M1 was produced by the hydration reaction of OPC and the pozzolanic activity of fly ash, however, in M3 the whole strength forming gel was produced by the pozzolanic activity of fly ash and slag.

In mix M7 the slag content was increased from 25% as in M3 to 30%, replacing a part of fly ash content but the hydrated lime content was kept the same. It showed 18.8, 13.4 and 12.5% improvement in the compressive strength results at the respective 7, 28 and 56 days of curing, in comparison to that of mix M3. This shows that the pozzolanic reactivity of slag was higher than that of fly ash, which has also been reported by other researchers [Nedeljković et al., 2018, Kuder et al., 2012]. This is most likely because of the following two reasons: (i) the mean particle size (D[4,3]) of slag was significantly lower than that of the fly ash that increases the surface area for the pozzolanic reactivity and (ii) the amorphous silica/aluminosilicate content of slag was significantly higher than that of the fly ash. The higher reactivity of slag in M7 was also visible in the increase in the C-S-H/C-A-S-H and C-A-H phases followed by higher consumption of the portlandite content compared to that of M3. Another important aspect that is to be noted is that where M3 showed similar strength as that of mix M1 at 7 days, M7 showed a small reduction in comparison to that of M5 (Fig. 8a). At 28 and 56 days of curing the increase in compressive strength of M7 vs M5 was lower than that of M3 vs M1 (Fig. 8). This shows that the negative effect of the replacement of OPC content with the equivalent amount of slag increases with the increase in the replacement level; however, within the upper range of 25 - 30% replacement levels the performance of slag was at par or better than that of the OPC. The SEM image showing the microstructure of M7 showed an improvement in the gel formation compared to that of M3; however, no considerable difference was observed compared to that of M5.

In mix M4, the FA content of M3 was partly replaced with 5% of nano-silica that brought about 100, 39.1, and 43.1% increase in its corresponding 7, 28 and 56-day compressive strength results, in comparison to that of mix M3. The TGA data shows a noticeable increase in the pozzolanic reactivity of M4 as evident in the increase in its C-S-H/C-A-S-H and C-A-H gel formations, and a significant increase in the consumption of its portlandite content at both 7 and 28days, compared to that of M3. To identify the relative benefit of partly replacing fly ash content of nano-silica, slag, fly ash and hydrated lime blended mix M4 with slag, the slag content was increased from 25% as in M4 to 30% in mix M8, keeping the remaining material composition the same. The compressive strength of M8 showed 17.4, 10.7 and 10.6% improvement at the respective curing ages of 7, 28 and 56 days, in comparison to that of mix M4. This was also reflected in the increase in the C-S-H/C-A-S-H and C-A-H gel formations supported by an increase in the consumption of the portlandite content of M8 in comparison to that of mix M4. This supports our previous observation that because of the higher surface area and amorphous silica/aluminosilicate content of slag the pozzolanic reactivity of slag is higher than that of fly ash. The SEM image of M8 did not show any considerable difference in the cement microstructure to that of mix M4, however, a noticeable increase in the strength forming gel was identified in nano silica modified mix M8 in comparison to that of mix M7 not comprising nano silica.

3.4. Concrete acid attack analysis

Fig. 9 shows the mass loss of concrete samples of various mix

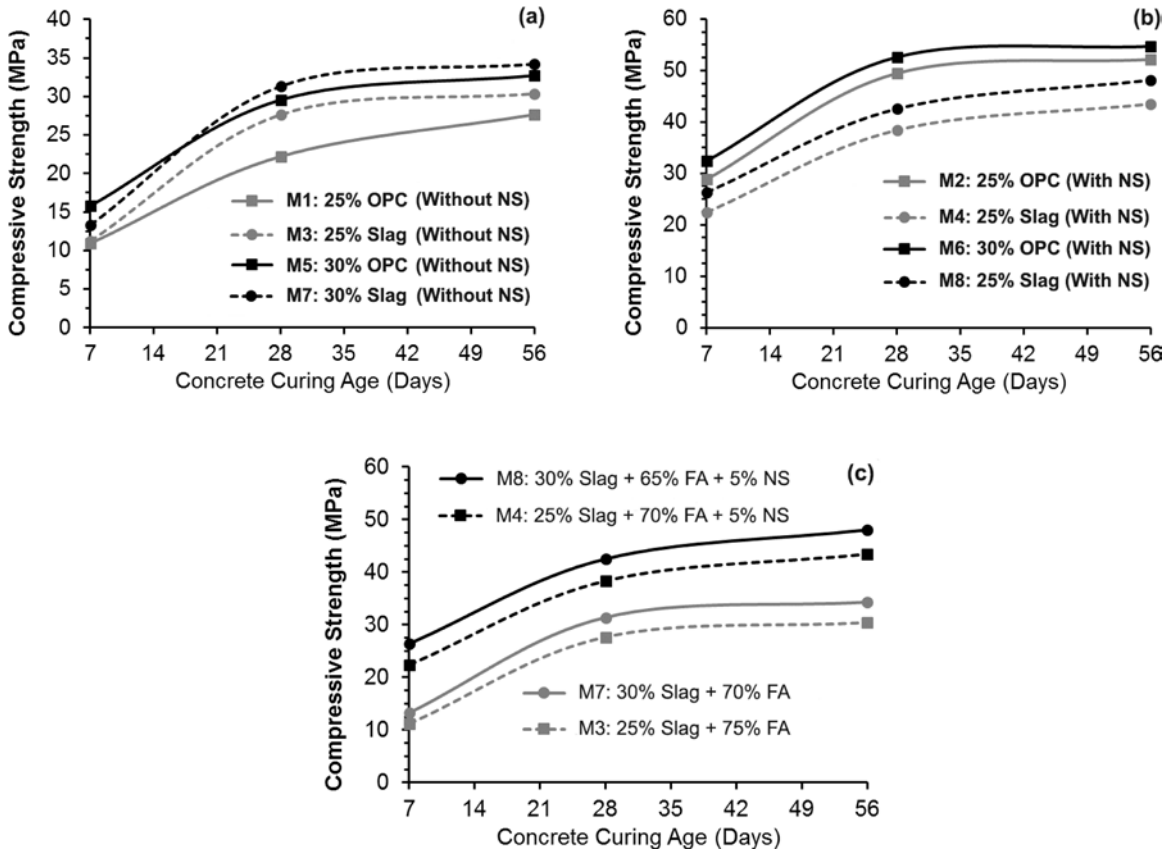

Fig. 8. Graphs showing (a) the effect of replacing OPC with slag in blended mixes not containing nano silica (b) the effect of replacing OPC with slag in blended mixes containing nano silica (c) the effect of an increase or decrease of slag and fly-ash on the compressive strength of concrete mixes

designs after keeping 28 and 56 days in 3.5% sulfuric acid solution. The control sample showed a significant mass loss at 28 days which significantly increased further at 56 days of soaking in 3.5% sulfuric acid solution. Similar observations were reported by Bassouni and Nehdi [Bassuoni and Nehdi, 2007]. This mass loss was also visible in the highly corroded picture of water washed control sample after 56 days of soaking in acid solution as shown in Fig. 10. Fig. 11 shows an off-white froth formation around the control sample at 56 days of soaking in sulfuric acid solution. It was collected and dried in an oven at 40 °C temperature for 24 hours before carrying out XRF and XRD analysis to ascertain its elemental and mineralogical composition. The XRD diffractogram shows various forms of calcium sulfate in addition to the presence of quartz. Table 7 shows the presence of a very large quantity of portlandite (CH_i) and calcite (CC_i) at 28 days of curing. Sulfuric acid reacts with portlandite and calcite to produce calcium sulfate as per the following equations:

$$Ca(OH)_2 + H_2SO_4 = => CaSO_4 + 2H_2O$$

$$CaCO_3 + H_2SO_4 = => CaSO_4 + CO_2\uparrow + 2H_2O$$

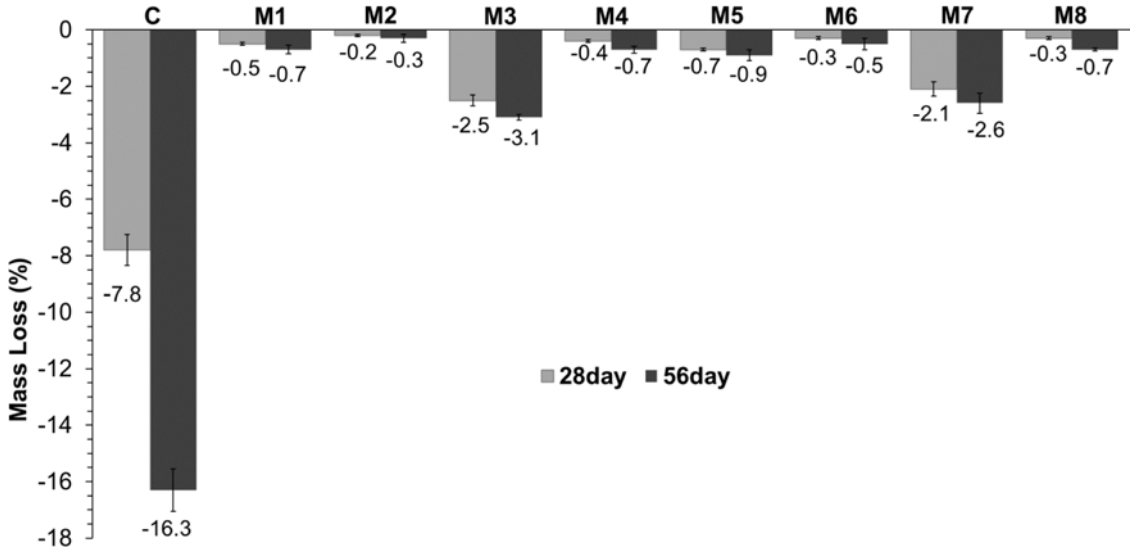

Fig. 9. Mass loss in concrete samples after 28 and 56 days of soaking in 3.5% sulphuric acid solution

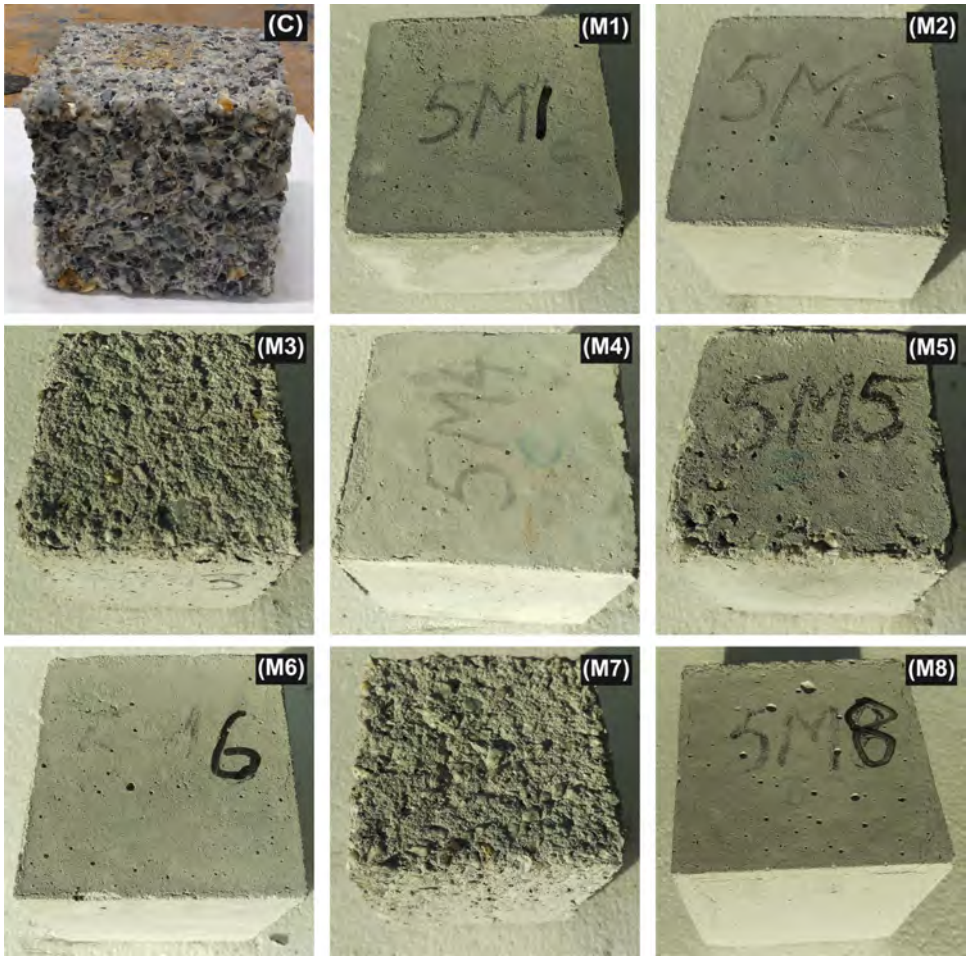

Fig. 10. Effect of soaking 28 day cured concrete samples in 3.5% sulfuric acid solution for an additional 56 days

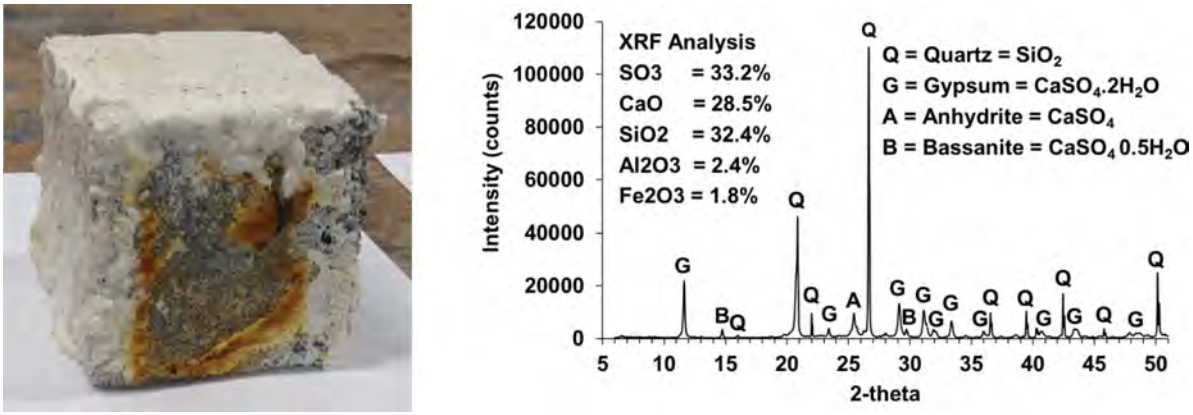

Fig. 11. Picture (left) showing the froth formation around the control sample kept in 3.5% sulfuric acid solution for 28 days and the graph on the right shows the XRD diffractogram of the froth along with its XRF analysis.

Table 7
Identified portlandite (CH_I), calcite (CC_I) and the calculated actual release of portlandite (CH_{ar}) from TGA analysis at 28 days of curing extracted from Table 6.

	C	M1	M2	M3	M4	M5	M6	M7	M8
CH_i % @ 28 days of curing	7.08	1.02	-	4.36	-	1.31	-	3.95	-
CC_i % @ 28 days of curing	10.90	3.91	2.30	6.33	6.19	5.05	2.67	5.69	5.48
CH_{ar} % @ 28 days of curing	15.15	3.91	1.70	9.04	4.58	5.05	1.98	8.16	4.06

The formation of froth around the control concrete sample was most likely because of the introduction of CO_2 gas into the large volume of calcium sulfate formed after the reaction of sulfuric acid with the portlandite and calcite content present in the sample. The quartz peak present in the XRD diffractogram of the froth material is most likely from the sand content dislodged from the concrete matrix. This is due to the volume expansion of the calcium sulfate produced by the reaction of sulfuric acid and portlandite/calcite phases, compared to the volume of the reactants (factor of 2.2), that induce tensile stresses within the cement matrix, resulting in cracking and spalling [Bassuoni and Nehdi, 2007, Monteny et al., 2001]. The XRF data of the froth content show a small amount of alumina and ferrite content, which most likely is produced from the cracking and spalling of the hydrated calcium aluminate and alumino-ferrite phases present in the cement matrix.

Mix M1 containing 25% OPC and 75% fly-ash showed a very small amount of mass loss compared to that of the control mix. Similar results were reported by Dinakar et al. [Dinakar et al., 2008]. This was also reflected in the picture of M1 (Fig. 10) that showed negligibly small damage to the concrete surface compared to that of the control sample. The portlandite and calcite contents present in M1 were significantly lower than that of the control sample at 28 days of curing when they were dipped in the acid solution. Even though the CH_{ar} content of M1 is approximately 26% of that of the control sample the mass loss was not proportionate to that of the control sample. The portlandite content of M1 was significantly lower than that of the control sample that most likely decreased its alkalinity thereby making the acid-base reaction less aggressive. Also, due to the lower portlandite and calcite contents present in M1 the resultant production of gypsum that expands in volume would also reduce significantly, thereby producing significantly less damaging effect compared to that of the control sample. With the increase in OPC content in M5 from 25 to 30% compared to that of M1, the resultant production of portlandite and calcite contents at 28 days of curing were also increased. This resulted in the increase in the production of gypsum thereby increasing the damage to the concrete sample of M5 compared to that of M1, which was also reflected in the corroded picture of M5 as shown in Fig. 10.

In mix M2 a part of FA content of M1 was replaced with 5% of amorphous nano silica, keeping the remaining material composition the same as that of M1. The portlandite content released by the hydration reaction of calcium silicates was totally consumed by the pozzolanic reaction of nano silica and fly ash, however a small amount of calcite was present at 28 days of curing as shown in Table 7. Similar observations of the significant increase in the consumption of the portlandite by the addition of nano silica were reported by Hou et al. [Hou et al., 2013] and, Shaikh and Hosan [Shaikh and Hosan, 2019]. Fig. 9 shows a negligibly small amount of mass loss in M2 that is most likely because of the reaction of the small amount of calcite present in the sample with the sulfuric acid solution. Very small micro scale surface damage was observed on the samples, which can be identified on zooming into the reduced sized picture of M2. On increasing the OPC content of the mix design from 25% in M2 to 30% in M6, even though the potential release of portlandite was higher because of the increase in OPC content it was all consumed by nano silica and fly ash present in the mix design. A small amount of calcite content was observed in M6 which was higher than that of M2 and contributed towards a small increase in its mass loss in comparison to that of M2. M6 showed small surface damage in the form of microcavities and surface cracking which again can be identified on zooming into the reduced-size picture of M6.

Mix M3 had a similar mix design as that of M1 but the OPC content present in M1 was replaced with slag in M3 and 15% hydrated lime was added as an external source of an alkaline material for the pozzolanic reaction. Our previous study [Roychand et al., 2018] shows that without an alkaline activator a cement composite containing low calcium fly ash and slag does not undergo any pozzolanic reaction to gain any structural strength, therefore, addition of an alkaline activator is a absolutely required. The total remaining portlandite at the end of 28 days of curing was 9.04% out of which 4.36% was present as portlandite and the remaining was converted to 6.33% of calcite. This large amount of portlandite and calcite content in M3 compared to that of M1 aggravated the damaging effect of the acid-base reaction on keeping the samples in the sulfuric acid solution. Fig. 9 shows a respective mass loss of 2.5 and 3.1% in M3 at 28 and 56 days of soaking periods in 3.5% sulfuric acid solution. This damage was also reflected in the sample condition picture of M3 as shown in Fig. 10. On further increasing the slag content from 25% in M3 to 30% in M7 the consumption of portlandite was increased. The remaining total portlandite was reduced to 8.16% which was present as 3.95% as portlandite and 5.69% as calcite content in M7. This reduction in remaining portlandite and calcite contents also reduced the damaging effect of acid-base reaction on M7, thereby reducing the mass loss to 2.1 and 2.6% compared to that of M3 at respective 28 and 56 days of acid soaking. The visual appearance of the damaged sample of M7 did not show any considerable difference compared to that M3 (Fig. 10) after 56 days of acid soaking.

In mix M4, the fly-ash content of M3 was partially substituted with 5% nano-silica keeping the remaining material composition the same. The addition of nano-silica accelerates the pozzolanic reaction [Roychand et al., 2016, Roychand et al., 2018, Björnström et al., 2004] consuming all the available portlandite content. The calcite content identified in M4 was slightly lower than that of M3. Since there was no free lime available in the system after 28 days of curing, this most likely reduced the pH of the cement matrix thereby lowering the aggravating effect of the acid-base reaction on keeping the sample in 3.5% sulfuric acid solution. The visual appearance of the damaged sample of M4 showed a significant improvement in the surface damage compared to that of M3 but it was similar to that of M2. Though the mass loss of M4 was slightly higher than that of M2 it was still very low in the overall damaging effect of the concrete samples kept in the acid solution. On further increasing the slag content from 25% in M4 to 30% in M8 the consumption of portlandite was increased and the remaining calcite content was also reduced. The presence of no portlandite significantly improves the performance of a concrete sample in an acid environment thereby reducing the aggravation of the acid base reaction; however, the presence of calcite content does induce some damaging effect on reacting with sulfuric acid. Although M8 showed a significant improvement over that of M7 (not containing nano silica), it did not show any considerable difference in both the mass loss as well as the visual concrete damage, after 56 days in acid solution, compared to that of M4 having a slightly lower amount of slag content.

4. Conclusions and recommendations for future work

C1) An environmental friendly zero cement concrete (M8) can be developed using multi-blended supplementary cementitious composites that surpasses ASTM's minimum strength requirement for concrete sewage pipes.

C2) Acid corrosion of concrete decreases with the decrease in free lime content however even the presence of calcite has a negative effect but to a very small degree compared to that of the portlandite. The negligible mass loss in the concrete samples containing no free lime but a small quantity of calcite shows that the strength forming C-S-H/C-A-S-H/C-A-H phases can stay unaffected in the acid environment if the concrete samples are free from portlandite and calcite contents.

C3) Higher the quantity of free lime available in the hardened cement concrete the worse is the aggravation of the acid-base reaction of the concrete samples in acid solution resulting in the increase in mass loss due to the acid corrosion of concrete.

C4) The zero-cement concrete so developed is highly effective in consuming all the free lime available in the system thereby making it highly durable in aggressive acid environments. The mass loss due to the corrosion of concrete from the acidic environment is improved significantly compared to that of OPC concrete making it highly effective for the manufacturing of concrete sewage pipes.

C5) Total consumption of free lime may also help in eliminating the effect of FOG calcification from the leaching of free lime present in cement matrix of OPC concrete pipes, that also leads to the clogging of sewage pipes.

R1) Recommendation number one for the future work is to look for ways to totally consume/eliminate both the free lime and calcite from the cement matrix to make the concrete sample completely resistant to acid corrosion.

R2) Recommendation number two for the future work is to carry out investigation of the long-term mechanical and durability properties of the design concrete mixes, simulating the real-world pH conditions.

CRediT authorship contribution statement

Rajeev Roychand: Conceptualization, Methodology, Investigation, Data curation, Formal analysis, Visualization, Writing - review & editing. **Jie Li:** Visualization, Writing - review & editing. **Saman De Silva:** Visualization, Writing - review & editing. **Mohammad Saberian:** Visualization, Writing - review & editing. **David Law:** Visualization, Writing - review & editing. **Biplob Kumar Pramanik:** Visualization, Writing - review & editing.

Declaration of Competing Interest

The authors declare that they have no known competing financial interests or personal relationships that could have appeared to influence the work reported in this paper.

References

Bongaarts, J., 2019. Special Report on Climate Change and Land Use. Intergovernmental Panel on Climate Change, 2018. Population and Development Review 45 (4), 936–937.

Andrew, R.M., 2018. *Global CO2 emissions from cement production*. Earth System Science Data 10 (1), 195–217.

Zuberi, M.J.S., Patel, M.K., 2017. Bottom-up analysis of energy efficiency improvement and CO2 emission reduction potentials in the Swiss cement industry. Journal of cleaner production 142, 4294–4309.

Talaei, A., Pier, D., Iyer, A.V., Ahiduzzaman, M., Kumar, A., 2019. Assessment of long-term energy efficiency improvement and greenhouse gas emissions mitigation options for the cement industry. Energy 170, 1051–1066.

Georgiopoulou, M., Lyberatos, G., 2018. Life cycle assessment of the use of alternative fuels in cement kilns: A case study. Journal of environmental management 216, 224–234.

Chatziaras, N., Psomopoulos, C.S., Themelis, N., 2016. Use of waste derived fuels in cement industry: a review. Management of Environmental Quality: an international journal,.

Roychand, R., De Silva, S., Law, D., Setunge, S., 2016. Materials, *Micro and nano engineered high volume ultrafine fly ash cement composite with and without additives*. International Journal of Concrete Structures and Materials 10 (1), 113–124.

Roychand, R., De Silva, S., Law, D., Setunge, S., 2016. High volume fly ash cement composite modified with nano silica, hydrated lime and set accelerator. Materials and Structures 49 (5), 1997–2008.

Roychand, R., De Silva, S., Setunge, S., Law, D., 2017. A quantitative study on the effect of nano SiO2, nano Al2O3 and nano CaCO3 on the physicochemical properties of very high volume fly ash cement composite. European Journal of Environmental and Civil Engineering 1–16.

Roychand, R., 2017. Performance of micro and nano engineered high volume fly ash cement composite. RMIT University, Melbourne, Australia.

Roychand, R., De Silva, S., Setunge, S., 2018. Nanosilica Modified High-Volume Fly Ash and Slag Cement Composite: Environmentally Friendly Alternative to OPC. Journal of Materials in Civil Engineering 30 (4), 04018043.

Jiang, Y., Ling, T.-C., Shi, C., Pan, S.-Y., 2018. Characteristics of steel slags and their use in cement and concrete—A review. Resources, Conservation and Recycling 136, 187–197.

Pedro, D., De Brito, J., Evangelista, L., 2017. *Evaluation of high-performance concrete with recycled aggregates: Use of densified silica fume as cement replacement*. Construction and Building Materials 147, 803–814.

Singh, N., Mithulraj, M., Arya, S., 2018. Influence of coal bottom ash as fine aggregates replacement on various properties of concretes: A review. Resources, Conservation and Recycling 138, 257–271.

Roychand, R., Pramanik, B.K., Zhang, G., Setunge, S., 2020. Recycling steel slag from municipal wastewater treatment plants into concrete applications–A step towards circular economy. Resources, Conservation and Recycling 152, 104533.

Islam, G.S., Rahman, M., Kazi, N., 2017. Waste glass powder as partial replacement of cement for sustainable concrete practice. International Journal of Sustainable Built Environment 6 (1), 37–44.

Lalitha, G., Sasidhar, C., Ramachandrudu, C., 2017. A review paper on strength and durability studies on concrete fine aggregate replaced with recycled crushed glass. International Journal of Civil Engineering and Technology 8 (2), 199–202.

Saberian, M., Li, J., Cameron, D., 2019. Effect of crushed glass on behavior of crushed recycled pavement materials together with crumb rubber for making a clean green base and subbase. Journal of Materials in Civil Engineering 31 (7), 04019108.

Saberian, M., Li, J., Perera, S.T.A.M., Ren, G., Roychand, R., Tokhi, H., 2020. An experimental study on the shear behaviour of recycled concrete aggregate incorporating recycled tyre waste. Construction and Building Materials 264, 120266.

Saberian, M., Li, J., 2018. Investigation of the mechanical properties and carbonation of construction and demolition materials together with rubber. Journal of cleaner production 202, 553–560..

Youssf, O., Hassanli, R., Mills, J.E., Skinner, W., Ma, X., Zhuge, Y., Roychand, R., Gravina, R., 2019. Influence of Mixing Procedures, Rubber Treatment, and Fibre Additives on Rubcrete Performance. Journal of Composites Science 3 (2), 41.

Abd-Elaal, E.-S., Araby, S., Mills, J.E., Youssf, O., Roychand, R., Ma, X., Zhuge, Y., Gravina, R.J., 2019. Novel approach to improve crumb rubber concrete strength using thermal treatment. Construction and Building Materials 229, 116901.

Roychand, R., Gravina, R.J., Zhuge, Y., Ma, X., Youssf, O., Mills, J.E., 2020. A comprehensive review on the mechanical properties of waste tire rubber concrete. Construction and Building Materials 237, 117651.

Hilton, B., Bawden, K., Winnebeck, K., Chandrasiri, C., Ariyachandra, E., Peethamparan, S., 2019. The functional and environmental performance of mixed cathode ray tubes and recycled glass as partial replacement for cement in concrete. Resources, Conservation and Recycling 151, 104451.

Madandoust, R., Ranjbar, M.M., Moghadam, H.A., Mousavi, S.Y., 2011. Mechanical properties and durability assessment of rice husk ash concrete. Biosystems engineering 110 (2), 144–152.

Aprianti, E., Shafigh, P., Bahri, S., Farahani, J.N., 2015. Supplementary cementitious materials origin from agricultural wastes–A review. Construction and Building Materials 74, 176–187.

Debbarma, S., Ransinchung, G., Singh, S., Sahdeo, S.K., 2020. Utilization of industrial and agricultural wastes for productions of sustainable roller compacted concrete pavement mixes containing reclaimed asphalt pavement aggregates. Resources, Conservation and Recycling 152, 104504.

Ashraf, M.S., Ghouleh, Z., Shao, Y., 2019. Production of eco-cement exclusively from municipal solid waste incineration residues. Resources, Conservation and Recycling 149, 332–342.

Juenger, M.C., Siddique, R., 2015. Recent advances in understanding the role of supplementary cementitious materials in concrete. Cement and Concrete Research 78, 71–80.

Gedam, B.A., Bhandari, N., Upadhyay, A., 2016. Influence of supplementary cementitious materials on shrinkage, creep, and durability of high-performance concrete. Journal of Materials in Civil Engineering 28 (4), 04015173.

Bastidas-Arteaga, E., Schoefs, F., 2015. Sustainable maintenance and repair of RC coastal structures. In: Proceedings of the Institution of Civil Engineers-Maritime Engineering. Thomas Telford Ltd.

Alexander, M., 2016. Marine concrete structures: design, durability and performance. Woodhead Publishing.

Wasim, M., Ngo, T.D., Abid, M., 2020. Investigation of long-term corrosion resistance of reinforced concrete structures constructed with various types of concretes in marine and various climate environments. Construction and Building Materials 237, 117701.

Wasim, M., Hussain, R.R., 2015. Passive film formation and corrosion initiation in lightweight concrete structures as compared to self compacting and ordinary concrete structures at elevated temperature in chloride rich marine environment. Construction and Building Materials 78, 144–152.

Mori, T., Nonaka, T., Tazaki, K., Koga, M., Hikosaka, Y., Noda, S., 1992. Interactions of nutrients, moisture and pH on microbial corrosion of concrete sewer pipes. Water research 26 (1), 29–37.

Mori, T., Koga, M., Hikosaka, Y., Nonaka, T., Mishina, F., Sakai, Y., Koizumi, J., 1991. Microbial corrosion of concrete sewer pipes, H2S production from sediments and determination of corrosion rate. Water Science and Technology 23 (7-9), 1275–1282.

Wells, T., Melchers, R.E., Bond, P., 2009. Factors involved in the long term corrosion of concrete sewers. In: Australasian corrosion association proceedings of corrosion prevention. Coffs Harbour, Australia. 11.

Wu, L., Hu, C., Liu, W.V., 2018. The sustainability of concrete in Sewer tunnel—A narrative review of acid corrosion in the city of Edmonton, Canada. Sustainability 10 (2), 517.

Oakes, K., 2019. Rise of the fatbergs. Elsevier.

Wallace, T., Gibbons, D., O'Dwyer, M., Curran, T.P., 2017. International evolution of fat, oil and grease (FOG) waste management–A review. Journal of environmental management 187, 424–435.

Wasim, M., Djukic, M.B., 2020. Long-term external microbiologically influenced corrosion of buried cast iron pipes in the presence of sulfate-reducing bacteria (SRB). Engineering Failure Analysis, 104657.

Hermansyah, H., Kubo, M., Shibasaki-Kitakawa, N., Yonemoto, T., 2006. Mathematical model for stepwise hydrolysis of triolein using Candida rugosa lipase in biphasic oil–water system. Biochemical Engineering Journal 31 (2), 125–132.

He, X., Francis Iii, L., Leming, M.L., Dean, L.O., Lappi, S.E., Ducoste, J.J., 2013. Mechanisms of fat, oil and grease (FOG) deposit formation in sewer lines. Water research 47 (13), 4451–4459.

Keener, K.M., Ducoste, J.J., Holt, L.M., 2008. Properties influencing fat, oil, and grease deposit formation. Water environment research 80 (12), 2241–2246.

The tip of the fatberg: Fatberg exhibit illustrates Melbourne's bigger wet wipe obsession. https://www.yvw.com.au/about-us/news-room/tip-fatberg-fatberg-exhibit-illustrates-melbournes-

bigger-wet-wipe-obsession Access date: 14-02-2010.
Williams, J., Clarkson, C., Mant, C., Drinkwater, A., May, E., 2012. Fat, oil and grease deposits in sewers: Characterisation of deposits and formation mechanisms. Water research 46 (19), 6319–6328.
Del Mundo, D.M.N., Sutheerawattananonda, M., 2017. Influence of fat and oil type on the yield, physico-chemical properties, and microstructure of fat, oil, and grease (FOG) deposits. Water research, 124, 308–319.
FOG Is The Biggest Cause Of Blocked Drains (2018). https://www.relinesolutions.com.au/pipe-relining-blog/fog-biggest-cause-of-blocked-drains access date: 23/02/2020.
Aydın, S., Yazıcı, H., Yiğiter, H., Baradan, B., 2007. Sulfuric acid resistance of high-volume fly ash concrete. Building and Environment, 42 (2), 717–721.
Torii, K., Kawamura, M., 1994. Effects of fly ash and silica fume on the resistance of mortar to sulfuric acid and sulfate attack. Cement and Concrete Research 24 (2), 361–370.
Jeon, J.-K., Moon, H.-Y., Ann, K.-Y., Kim, H.-S., Kim, Y.-B., 2006. Effect of ground granulated blast furnace slag, pulverized fuel ash, silica fume on sulfuric acid corrosion resistance of cement matrix.. International Journal of Concrete Structures and Materials 18 (2E), 97–102.
Mahdikhani, M., Bamshad, O., Shirvani, M.F., 2018. Mechanical properties and durability of concrete specimens containing nano silica in sulfuric acid rain condition. Construction and building materials 167, 929–935.
Deb, P.S., P.K. Sarker, and S. Barbhuiya, *Sorptivity and acid resistance of ambient-cured geopolymer mortars containing nano-silica*. Cement and Concrete Composites, 2016.72: p. 235-245.
Kusum, S.A., Pour-Ghaz, M., Ducoste, J., 2018. Evaluating Alternative Binder Materials for Sewer Collection System Concrete Structures to Reduce Fat, Oil, and Grease Related Sanitary Sewer Overflows. In: Proceedings of the Water Environment Federation. 2018. pp. 258–266.
Xie, Y., Lin, X., Pan, W., Ji, T., Liang, Y., Zhang, H., 2018. Study on corrosion mechanism of alkali-activated concrete with biogenic sulfuric acid. Construction and Building Materials 188, 9–16.
Li, Z., Peethamparan, S., 2018. Leaching resistance of alkali-activated slag and fly ash mortars exposed to organic acid. Green Materials 6 (3), 117–130.
ASTM International. C76M-19b *Standard Specification for Reinforced Concrete Culvert, Storm Drain, and Sewer Pipe (Metric)*. West Conshohocken, PA; ASTM International, 2019. doi: https://doi.org/10.1520/C0076M-19B.
Vincke, E., Boon, N., Verstraete, W., 2001. Analysis of the microbial communities on corroded concrete sewer pipes–a case study. Applied Microbiology and Biotechnology 57 (5-6), 776–785.
Kim, Y.-Y., Lee, K.-M., Bang, J.-W., Kwon, S.-J., 2014. Effect of W/C ratio on durability and porosity in cement mortar with constant cement amount. Advances in Materials Science and Engineering 2014.
Nkinamubanzi, P.-C., Mantellato, S., Flatt, R., 2016. *Superplasticizers in practice*, in *Science and technology of concrete admixtures*. Elsevier, pp. 353–377.
Sonebi, M., García-Taengua, E., Hossain, K., Khatib, J., Lachemi, M., 2015. Effect of nanosilica addition on the fresh properties and shrinkage of mortars with fly ash and superplasticizer. Construction and Building Materials 84, 269–276.
AS 1012.8.1: 2014 *Methods of testing concrete - Method for making and curing concrete - Compression and indirect tensile test specimens*. Standards Australia Ltd., GPO Box 476, Sydney, NSW 2001, Australiawww.standards.org.au.
AS 1012.9:2014, *Compressive strength tests - Concrete, mortar and grout specimens*. Standards Australia Ltd., GPO Box 476, Sydney, NSW2001, Australiawww.standards.org.au.
Sar, E., 2018. Low Carbon Technology Roadmap for the Indian Cement Sector: Status Review, in: Fonta, P. (Ed.). World Business Council for Sustainable Development.
Scrivener, K., Snellings, R., Lothenbach, B., 2016. A practical guide to microstructural analysis of cementitious materials 540 Crc Press, Boca Raton.
Şahmaran, M., Yaman, İ.Ö., Tokyay, M., 2009. Transport and mechanical properties of self consolidating concrete with high volume fly ash. Cement and concrete composites 31 (2), 99–106.
Liu, M., 2010. Self-compacting concrete with different levels of pulverized fuel ash.. Construction and Building Materials 24 (7), 1245–1252.
Midgley, H., Pettifer, K., 1971. The micro structure of hydrated super sulphated cement. Cement and Concrete Research 1 (1), 101–104.
Yan, P., Yang, W., Qin, X., You, Y., 1999. Microstructure and properties of the binder of fly ash-fluorogypsum-Portland cement. Cement and concrete research 29 (3), 349–354.
Zhang, M.-H., Islam, J., 2012. Use of nano-silica to reduce setting time and increase early strength of concretes with high volumes of fly ash or slag. Construction and Building Materials 29, 573–580.
Hou, P.-k., Kawashima, S., Wang, K.-j., Corr, D.J., Qian, J.-s., Shah, S.P., 2013. Effects of colloidal nanosilica on rheological and mechanical properties of fly ash–cement mortar. Cement and Concrete Composites 35 (1), 12–22.
Björnström, J., Martinelli, A., Matic, A., Börjesson, L., Panas, I., 2004. Accelerating effects of colloidal nano-silica for beneficial calcium–silicate–hydrate formation in cement. Chemical Physics Letters 392 (1-3), 242–248.
Singh, L., Karade, S., Bhattacharyya, S., Yousuf, M., Ahalawat, S., 2013. Beneficial role of nanosilica in cement based materials–A review. Construction and Building Materials 47, 1069–1077.
Zhang, B., Tan, H., Shen, W., Xu, G., Ma, B., Ji, X., 2018. Nano-silica and silica fume modified cement mortar used as Surface Protection Material to enhance the impermeability. Cement and Concrete Composites 92, 7-17.
Nedeljković, M., Li, Z., Ye, G., 2018. Setting, strength, and autogenous shrinkage of alkali-activated fly ash and slag pastes: Effect of slag content. Materials 11 (11), 2121.
Kuder, K., Lehman, D., Berman, J., Hannesson, G., Shogren, R., 2012. Mechanical properties of self consolidating concrete blended with high volumes of fly ash and slag. Construction and Building Materials 34, 285–295.
Bassuoni, M., Nehdi, M., 2007. Resistance of self-consolidating concrete to sulfuric acid attack with consecutive pH reduction. Cement and Concrete Research 37 (7), 1070–1084.
Monteny, J., De Belie, N., Vincke, E., Verstraete, W., Taerwe, L., 2001. Chemical and microbiological tests to simulate sulfuric acid corrosion of polymer-modified concrete. Cement and Concrete Research 31 (9), 1359–1365.
Dinakar, P., Babu, K., Santhanam, M., 2008. Durability properties of high volume fly ash self compacting concretes. Cement and Concrete Composites 30 (10), 880–886.
Shaikh, F.U., Hosan, A., 2019. High Volume Slag and Slag-Fly Ash Blended Cement Pastes Containing Nano Silica. Materials Science Forum Trans Tech Publ.